Blood Speckle-Tracking Based on High–Frame Rate Ultrasound Imaging in Pediatric Cardiology

Siri A. Nyrnes, MD, PhD, Solveig Fadnes, MSc, PhD, Morten Smedsrud Wigen, MSc, PhD, Luc Mertens, MD, PhD, and Lasse Lovstakken, MSc, PhD, *Trondheim, Norway; and Toronto, Ontario, Canada*

Background: Flow properties play an important role in cardiac function, remodeling, and morphogenesis but cannot be displayed in detail with today's echocardiographic techniques. The authors hypothesized that blood speckle-tracking (BST) could visualize and quantify flow patterns. The aim of this study was to determine the feasibility, accuracy, and potential clinical applications of BST in pediatric cardiology.

Methods: BST is based on high–frame rate ultrasound, using a combination of plane-wave imaging and parallel receive beamforming. Pattern-matching techniques are used to quantify blood speckle motion. Accuracy of BST velocity measurements was validated using a rotating phantom and by comparing BST-derived inflow velocities with pulsed-wave Doppler obtained in the left ventricles of healthy control subjects. To test clinical feasibility, 102 subjects (21 weeks to 11.5 years of age) were prospectively enrolled, including healthy fetuses (n = 4), healthy control subjects (n = 51), and patients with different cardiac diseases (n = 47).

Results: The phantom data showed a good correlation (r = 0.95, with a tracking quality threshold of 0.4) between estimated BST velocities and reference velocities down to a depth of 8 cm. There was a good correlation (r = 0.76) between left ventricular inflow velocity measured using BST and pulsed-wave Doppler. BST displayed lower velocities (mean ± SD, 0.59 ± 0.14 vs 0.82 ± 0.21 m/sec for pulsed-wave Doppler). However, the velocity amplitude in BST increases with reduced smoothing. The clinical feasibility of BST was high, as flow patterns in the area of interest could be visualized in all but one case (>99%).

Conclusions: BST is highly feasible in fetal and pediatric echocardiography and provides a novel approach for visualizing blood flow patterns. BST provides accurate velocity measurements down to 8 cm, but compared with pulsed-wave Doppler, BST displays lower velocities. Studying blood flow properties may provide novel insights into the pathophysiology of pediatric heart disease and could become an important diagnostic tool. (J Am Soc Echocardiogr 2020;33:493-503.)

Keywords: Blood speckle-tracking, Blood speckle-imaging, Cardiac flow properties, High–frame rate ultrasound imaging

From the Department of Circulation and Medical Imaging, Norwegian University of Science and Technology (S.A.N., S.F., M.S.W., L.L.), the Children's Clinic, St. Olavs Hospital, Trondheim University Hospital (S.A.N.), Trondheim, Norway; and the Department of Cardiology, The Hospital for Sick Children, University of Toronto, Toronto, Ontario, Canada (L.M.).

This work was supported by the Joint Research Committee between St. Olavs Hospital and the Faculty of Medicine, Norwegian University of Science and Technology (2014/23203), and the Research Council of Norway (RCN 230455 and RCN 237887, the latter through the Centre for Innovative Ultrasound Solutions).

Conflicts of interest: Dr. Lovstakken has and Dr. Wigen has had a part-time consultancy in GE Vingmed Ultrasound.

Reprint requests: Siri A. Nyrnes, MD, PhD, Department of Circulation and Medical Imaging, Norwegian University of Science and Technology, Olav Kyrresgt. 9, 7489 Trondheim, Norway (E-mail: *siri.a.nyrnes@ntnu.no*).

0894-7317

https://doi.org/10.1016/j.echo.2019.11.003

Congenital heart defects are associated with significant alterations in blood flow patterns and intracardiac hemodynamics. Direct visualization of complex flow patterns could therefore be important for diagnosis, understanding of pathophysiology, and prediction of outcomes. Our group has recently demonstrated that high–frame rate ultrasound with blood speckle-tracking (BST) can be used to quantify, visualize, and analyze complex flow patterns.[1,2]

During fetal development, blood flow patterns in the developing heart have been proposed to influence cardiac morphogenesis,[3] and intracardiac hemodynamics have been identified as a key factor in cardiovascular development.[4,5] Vortex flow, which is a circular or elliptical rotating mass of fluid, has been suggested to play an important role in cardiac function.[6,7] Intraventricular vortex properties and associated energetic efficiencies influence patient outcomes[8,9] and provide new pathophysiologic insights in disease progression.[10]

Several approaches to advanced flow imaging have been introduced, including phase-contrast cardiac magnetic resonance imaging and contrast-enhanced ultrasound (echocardiographic particle image velocimetry [EPIV]).[11,12] Neither of these approaches is well

Abbreviations

BST = Blood speckle-tracking

CDI = Color Doppler imaging

EL = Energy loss

EPIV = Echocardiographic particle image velocimetry

KE = Kinetic energy

LV = Left ventricular

PRF = Pulse repetition frequency

PW = Pulsed-wave

ST = Speckle-tracking

TQ = Tracking quality

VFM = Ultrasound vector flow mapping

VO = Vorticity

VSD = Ventricular septal defect

suited for younger children, because of their long acquisition times (cardiac magnetic resonance imaging) and more invasive nature (contrast infusion in EPIV). Ultrasound vector flow mapping (VFM) combines color Doppler imaging (CDI) with endocardial wall motion analysis to estimate the lateral velocity component.[13] This method has been applied in children.[14] Three-dimensional vector Doppler imaging merges three-dimensional color Doppler images from different acoustic windows and has been used to visualize three-dimensional intracardiac flow dynamics in pediatric patients,[15] but it depends on sufficient image overlap and accurate image registration.

The recent development of high–frame rate ultrasound allows a new approach to blood flow assessment. BST is based on ultrafast ultrasound imaging,[16] as high frame rates are needed to track blood flow.[1] The speckle-tracking features are similar to those used in tissue speckle-tracking, used to study myocardial deformation.[17] BST provides a direct measurement of blood velocity vectors, without requiring contrast agents or physical assumptions. However, the accuracy and feasibility of these new technologies are still unclear.[18] In this study, we describe the BST technique, its validation, and its feasibility, and we discuss potential clinical applications on the basis of selected patient examples.

METHODS

Blood Speckle-Tracking

BST is a flow-imaging technique combining high–frame rate imaging capabilities with image pattern matching (speckle-tracking) to directly measure and visualize blood vector velocity fields. The ultrasound speckle pattern inside the vessels and cardiac chambers is extracted by attenuating the stronger tissue echoes using a wall filter. Visualization of the blood speckle movement was the first step in the development of BST.[19] Computer tracking of the speckle movement requires high frame rates (in the kilohertz range), which are achieved by emitting broader ultrasound pulses that cover a wider spatial imaging region and by generating several image lines in parallel for each emitted pulse. Without considering real-time processing limitations, it is possible to acquire data from the full image region for each emitted pulse, resulting in thousands of sector images per second.[16] With frame rates in the kilohertz range, it is possible to use pattern-matching techniques to quantify the movement of blood speckles directly, without the use of contrast agents.[1,20]

Because of current real-time processing limitations, we were limited to 16 image lines in parallel, and we used a limited number of transmit pulses (three to nine) for every image frame, each covering a small image region of interest. An ensemble of unfocused pulses was emitted for each region (transmit direction) to track the blood speckle. The high–frame rate setup used for BST acquires image data at the Doppler pulse repetition frequency (PRF). However, because we have a duplex imaging setup, the flow acquisition is interrupted by B-mode image acquisition at regular intervals. One blood velocity measurement is averaged for each duplex flow acquisition (i.e., *n* images acquired at the Doppler PRF), and this gives a velocity measurement rate equal to the duplex display frame rate, which was 30–60 Hz in this study, depending on the color region of interest, depth, and width. This duplex setup is like a color Doppler acquisition.

In BST, we define a small image kernel in the first image and search for the same speckle signature in the following frame (Figures 1A and 1B). This is then repeated for a grid of measurements. In this way, the velocity and direction of the blood flow can be quantified.[1] Tracking quality (TQ) is a measure of the difference in correlation between the best match and the alternative matches in a search area (Figures 1A–1D). The tracking result selected as the best match has the highest correlation with the speckle signature in the previous frame. To be confident that it is a valid result, it should also be significantly different from the alternative matches. Figures 1C and 1D illustrate high and low TQ, respectively. A distinct difference between the best match and the alternative matches results in a high TQ value (Figure 1C).

In our study, BST was further combined with CDI, so that the radial velocity measurement was provided from color Doppler, and the lateral velocity estimate only was determined by tracking. This approach reduces computation time as well as measurement variance.[2] BST processing consists of initial wall filtering, followed by the tracking algorithm. Finally, data smoothing in space and time is used to reduce variance (3-5 mm [x,z], 40 msec).

The angle-independent blood velocity measurements can be visualized as arrows, streamlines, or path lines with or without underlying CDI, thereby highlighting areas of complex flow. BST also allows the measurement of quantitative flow measures, such as velocity magnitude, vorticity (VO), energy loss (EL), and kinetic energy (KE). EL is related to the viscous losses due to shear motion of the fluid,[13] while KE has been introduced as a useful parameter for assessing the ejection of blood flow from the left ventricle.[21] VO is a parameter calculated through the curl of the velocity vector field and represents the local spinning motion (angular velocity) in the flow field.[22] Current definitions and equations are found in the Supplemental Material.[21]

Patient Selection

This study was conducted at the Norwegian University of Science and Technology and St. Olavs University Hospital in Trondheim, Norway, where participant recruitment was done in parallel with continuous method development. The Regional Committee for Medical and Health Research Ethics, REC Central, approved the study (2010/499). Inclusion criteria were referral for echocardiography, age <12 years, and written informed consent from the parents. Patients were recruited between August 2010 and January 2018. A pediatric cardiologist (S.A.N.) performed the echocardiographic examinations, occasionally together with the engineers developing the technique. In total, 102 subjects were included: 51 normal control subjects (ranging in age from 2-day-old term neonates to 10-year-old children), 47 cardiac patients (age range, 1 day to 11.5 years), and four healthy fetuses (21, 24, 29, and 29 weeks of age).

Equipment, Image Acquisition, and Processing

Images were acquired using a Vivid E9 system (GE Vingmed Ultrasound, Horten, Norway), modified with research software to

HIGHLIGHTS

- BST is based on high–frame rate ultrasound.
- BST provides new information on blood flow patterns.
- BST is feasible in fetuses and children.
- BST TQ is high down to 8-cm depth.

acquire plane-wave ultrasound images. We used the linear 9L probe and the 6S and 12S phased-array probes (GE Healthcare, Milwaukee, WI).

The participants underwent routine clinical echocardiography before the study images were obtained. Participants with normal findings on echocardiographic examination were recruited as control subjects. The BST data were acquired on the research scanner, which included storage of the raw in-phase and quadrature data required for the offline use of the speckle-tracking algorithm. During acquisition, CDI was displayed in real time, optionally with added real-time speckle visualization.[19] Data were digitally stored for offline processing using in-house-developed software.

Accuracy of the Velocity Estimates In Vitro and In Vivo

Previous validation of BST in technical publications is summarized in Supplemental Table 1.[1,2,20,23-25] In this work, we further validated pediatric BST on the basis of images obtained with a 6 MHz phased-array probe and using an in-house-made rotating tissue-mimicking phantom with a known velocity profile. The phantom had a constant angular velocity (285 rounds/min), resulting in a span of velocities within the phantom between 0 m/sec at the center and 1.5 m/sec at the edges. The imaging was performed in a water bath through a silicon acoustic window. The tracking grid had a resolution of 1 mm^2, giving 180 × 130 tracking estimates for each frame, where 61 frames were used for analysis. Ten thousand randomly selected points from these estimates within the phantom were plotted after postprocessing (smoothing). Furthermore, for all control subjects, the maximum left ventricular (LV) inflow velocities measured by BST were compared with the pulsed-wave (PW) Doppler measurements in the mitral valve for all control subjects.

A TQ value (equation given in the Supplemental Material) was calculated for each individual measurement. The TQ map grades the expected tracking accuracy and was scaled from 0 to 1, where 1 represents perfect tracking and 0 represents very poor tracking. The relation between the true tracking accuracy and TQ was validated in vitro in the rotating phantom. The tracking accuracy was further evaluated in vivo by measuring the average TQ in the LV four-chamber view in the healthy pediatric control subjects ($n = 51$). Furthermore, the general TQ in all standard views was subjectively evaluated as good, fair, or poor.

Statistical Analysis

Data for continuous variables are presented as mean ± SD if normally distributed or as median and interquartile range if not normally distributed. Paired-samples *t* tests were used to compare BST and PW Doppler measurements, as the differences between groups were approximately normally distributed. Linear regression analysis was used to examine the relationship between the reference velocities and the BST velocities in the flow phantom. Linear regression analyses were also performed to examine the relationships between TQ and heart rate, between TQ and age, and among VO, EL, KE, and age. The values are presented in scatterplots, including regression lines with 95% CIs. The in vitro scatterplot and linear regression analysis was performed using MATLAB (The MathWorks, Natick, MA). The in vivo scatterplots and linear regression analyses were conducted using Python with the Statsmodels package for regression analyses and the Seaborn library for visualization. The remaining statistical analyses were performed using IBM SPSS Statistics version 25.0 (IBM, Armonk, NY).

RESULTS

The results from validation, accuracy, and clinical feasibility testing of BST in this study are summarized in Table 1.

BST Validation and TQ In Vitro

Using the rotating tissue-mimicking phantom for the 6S probe, we studied the BST TQ at different TQ thresholds. Supplemental Table 2 displays the BST quality regression analysis for the different TQ thresholds. On the basis of these results, we categorized agreement as follows: TQ > 0.5 ≈ excellent, TQ > 0.3 to 0.5 ≈ good, TQ > 0.2 to 0.3 ≈ fair, and TQ < 0.2 ≈ poor. A high TQ cutoff leads to fewer data to analyze (Supplemental Table 2). Figure 2 displays the results from the rotating tissue-mimicking phantom and demonstrates good agreement between the BST velocity measurements and the ground truth down to a depth of 8 cm. The regression line displayed

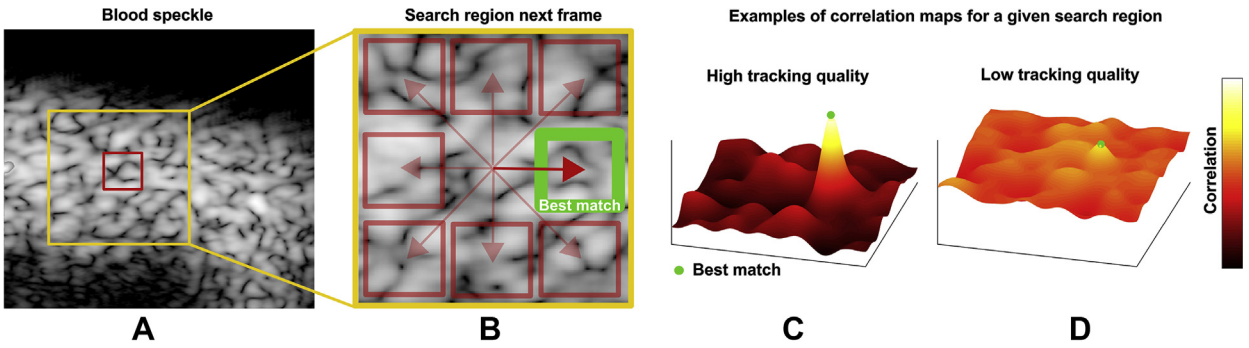

Figure 1 Speckle-tracking and TQ. A kernel is defined in the first frame **(A)**, and the best match of this kernel is searched for in the next frame **(B)**. If the best match can be clearly distinguished from the alternative matches, as shown in **(C)**, the TQ is high. In contrast, if there is little difference between the best match and the alternative matches, the TQ is low **(D)**.

Table 1 Validation, accuracy, and clinical feasibility of BST in pediatric cardiology

Test	Main results	Full details
In vitro		
Rotating tissue-mimicking phantom: 6S probe, maximum velocity 1.5 m/sec	Correlation: estimated vs reference velocity <8 cm, good; 8–10 cm, fair; >10 cm, poor. Accurate velocity estimates 3 times above the Nyquist limit (0.5 m/sec). TQ > 0.5 ≈ excellent, TQ 0.3–0.5 ≈ good, TQ 0.2–0.3 ≈ fair, TQ < 0.2 ≈ poor.	Figure 2, Supplemental Table 2
Rotating tissue-mimicking phantom: 6S probe, validation of TQ maps	Good correlation between TQ and accuracy of the velocity measurements. For TQ threshold 0.4: $y = 0.95 \times x + 0.02$, where y is BST velocity estimate and x is ground truth.	Figure 2, Supplemental Table 2
In vivo	First clinical feasibility study	
BST compared with PW Doppler in PV, corresponding TQ map	ST velocity estimates showed good correspondence with the PW Doppler spectrum.	Figure 4
LV velocity during inflow measured by BST compared with PW Doppler in MV	BST underestimates velocities compared with the PW envelope, but there is good correlation ($r = 0.76$) between the methods.	Figure 3A, Table 2
TQ maps of the LV four-chamber view in 51 healthy pediatric control subjects	Mean TQ 0.43 ± 0.06, corresponding to a correlation coefficient of >0.95 according to results from the flow phantom.	Figures 3B and 3C and Figure 5 (LV segmentation), Tables 2 and 3
Feasibility	High (>99%), as BST visualized flow patterns in the area of interest in all but one case.	Figures 4-10 and Supplemental Figures 1 and 2, Table 2
Potential clinical value	Selected clinical examples demonstrating potential clinical value.	Figures 6-8 and 10, Supplemental Figures 1 and 2

MV, Mitral valve; *PV*, pulmonary valve; *ST*, speckle-tracking.

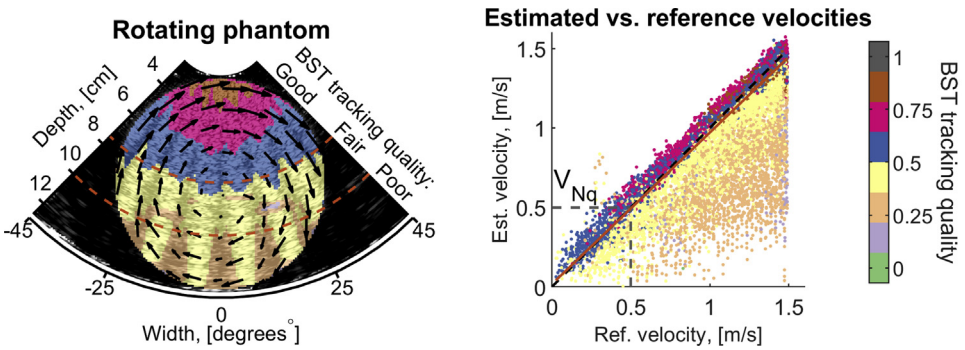

Figure 2 In vitro rotating phantom validation of the 6S probe. The figure of the phantom to the left shows the TQ as a function of the depth. The TQ is acceptable down to a depth of 8 cm. The graph on the *right* shows the agreement of the BST velocity measurements with the reference velocity and the corresponding TQ map. All estimates are colored according to their TQ value. The *orange regression line* corresponds to a TQ cutoff of 0.4 ($r = 0.95$).

in Figure 2 corresponds to TQ ≥ 0.4, yielding a coefficient of correlation (r) of 0.95.

BST Feasibility, Accuracy, and TQ In Vivo

The cardiac patients included a variety of pediatric and congenital heart diseases, including ventricular and atrial septal defects, valve stenosis, complex heart defects, pulmonary hypertension, and cardiomyopathies. Demographics, echocardiographic results, and technical specifications for the healthy control subjects are presented in Table 2. The BST method managed to quantify and visualize flow patterns in the area of interest in all patients except one.

The first 33 neonates were examined using only a linear probe (9L). Despite the wider footprint, it was possible to obtain images from all standard views in newborn patients. The method was improved in parallel with patient inclusion, and in the next 69 subjects, we were also able to use the same technique for phased array probes (12S and 6S). We preferred phased-array probes for all views

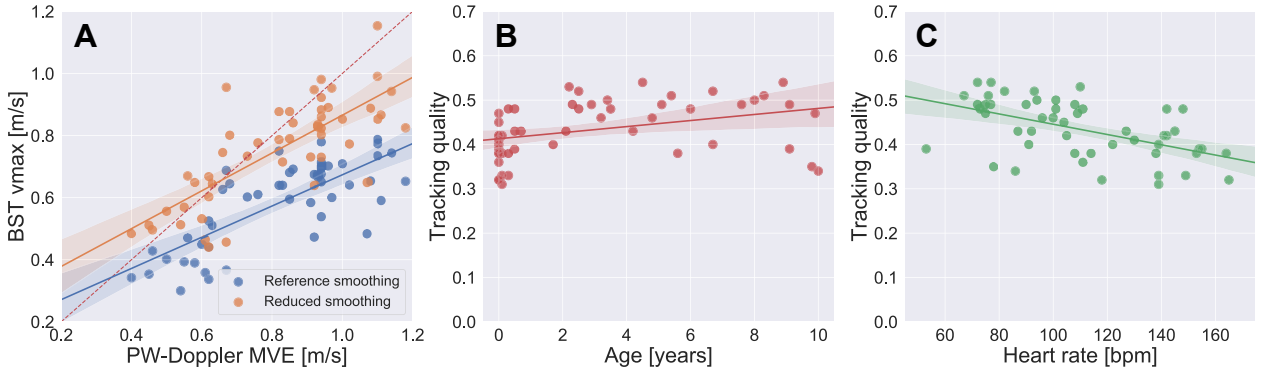

Figure 3 BST accuracy and TQ in the left ventricle. Analysis from 51 healthy control subjects. The scatterplots display correlations, the regression lines are shown as colored lines with 95% CIs (*shadowed lines*). **(A)** Speckle-tracking maximum velocity during inflow vs the PW Doppler mitral valve E velocity. The *blue line* represents velocity measurements using the chosen reference smoothing setting (5 mm × 5 mm × 40 msec), while the *orange line* represents measurements with reduced smoothing settings (3 mm × 3 mm × 0 msec). The *red dotted line* represents complete agreement. **(B)** TQ vs age. **(C)** TQ vs heart rate and shows that the average TQ is lower at high heart rates.

in children >1 year of age because of depth limitations. Technical comparison between BST in linear (9L) versus phased-array (6S) transducers has been previously published.[20]

A scatterplot displaying the correlation between the speckle-tracking maximum velocity during inflow and the PW Doppler mitral valve E velocity is shown in Figure 3A. This figure shows that BST measures lower LV inflow velocities compared with PW Doppler in vivo and that the difference tends to increase with higher velocities. The reference smoothing (5 mm × 5 mm × 40 msec) was chosen to give a good qualitative visualization of flow patterns with limited noise artifacts. By analyzing the BST data with reduced smoothing settings (3 mm × 3 mm × 0 msec), the BST velocity estimates are more like PW Doppler (Figure 3A), but this leads to more noise artifacts. The mean LV TQ in the control group was 0.43, corresponding to a correlation coefficient of >0.95, according to the experiments with the flow phantom (Supplemental Table 2). The TQ decreased with higher heart rates (Figure 3C, Table 3) and was not significantly correlated with age (Figure 3C, Table 3). TQ had a statistically significant correlation with PRF ($r = 0.58$). For the control subjects, the subjective TQ was classified as good in 34 cases, fair in 15 cases, and poor in two cases. For the pilot fetal examinations, the image quality of the linear-array probe and 6S phased-array probe was fair (4–5 cm in depth). For the whole study group in general, low TQ was seen regionally in cases of partial wall filter dropouts, substantial out-of-plane blood motion, and areas close to the valves and endocardial border (high clutter levels).

Figure 4 shows an example of the in vivo TQ in the main pulmonary artery using the 12S probe. The figure illustrates a good agreement between the BST and PW Doppler velocities (separate recordings). A corresponding TQ map illustrates that the TQ is best centrally in the image and decreases with increasing depth, as expected.

Figure 5 demonstrates LV BST flow in a healthy 9-year-old child. The image on the left illustrates a physiologic midventricular vortex. The TQ map (middle image) demonstrates that the TQ is best near the probe. However, valid estimates are seen down to 8 cm in depth. For dropout regions due to wall filtering, velocity fields can optionally be reconstructed by including wall motion information,[24] similar to that used in VFM, as shown on the right in Figure 5. In this example, a lateral vortex above the mitral valve is better displayed (Figure 5, Supplemental Video 1 available at www.onlinejase.com).

Selected Patient Examples

We selected case examples to illustrate how BST could be used in clinical practice. As the visual impression of BST is better when looking at videos compared with single frames, each example is linked to videos that demonstrate the BST technique using a particle animation technique.[25]

Advanced Flow Visualization

BST provides new ways of imaging flow, which include detailed visualization of more complex flow patterns. Left and right ventricular flow patterns in a healthy child are illustrated in Supplemental Figures 1 and 2. Compared with the underlying CDI flow map, more details regarding flow features, including visualization of vortices in the ventricles, are shown. The normal flow patterns are important as a point of reference for children with heart disease. This is demonstrated in Figure 6 and Supplemental Videos 2 and 3 (available at www.onlinejase.com), which compare the normal laminar pulmonary artery flow in a healthy neonate with the persistent abnormal vortex formation in the pulmonary artery in a neonate with pulmonary hypertension.

Figure 7 and Supplemental Videos 4 and 5 (available at www.onlinejase.com) demonstrate that BST is feasible for visualization of detailed blood flow patterns in the fetus, demonstrating flow in the aortic arch and descending aorta (9L probe) and in the four-chamber view (6S probe). The particle visualization of the normal circulation in a 24-week-old fetus demonstrates detailed visualization of flow in the aorta. The four-chamber view of a 29-week-old fetus demonstrates vortex formation in the left and right ventricles that is poorly demonstrated by CDI alone.

Quantitative Flow Properties

In the following selected examples, we present cases in which cardiac BST is used to display flow properties such as VO, EL, and KE. VO is defined as local rotation of blood or mathematically as the curl of the

Table 2 Demographics, echocardiography, and technical specifications: healthy control subjects

Demographics healthy control subjects (*N* = 51)	Value
Age, y	2.2 (0.1–5.6)
Sex, female/male	28/23
BSA, m^2	0.58 ± 0.33
Echocardiography	
TQ	0.43 ± 0.06
MVE maximum (PW Doppler envelope), m/sec	0.82 ± 0.21
Mean LV maximum inflow velocity (BST1), m/sec	0.59 ± 0.14
Mean LV maximum inflow velocity (BST2), m/sec	0.76 ± 0.17
Mean LV maximum VO (BST1), Hz	40.47 ± 9.47
Mean LV maximum EL (BST1), mW/m	9.87 ± 6.77
Mean LV maximum KE loss (BST1), J/m	0.07 ± 0.06
FS, %	36.34 ± 4.18
HR in the defined cardiac cycle, beats/min	110 ± 29
Technical specifications	
Probe used, 6S/12S	33/18
PRF = tracking frame rate, Hz	5,725 ± 940
Transmit pulses	3–9
Parallel receive lines	16
File size, MB	86.37 ± 27.4

Data are expressed as mean ± SD, median (interquartile range), or number. BST1: analysis with the reference smoothing setting (5 mm × 5 mm × 40 msec). BST2: analysis with reduced smoothing setting (3 mm × 3 mm × 0 msec). Subjects analyzed were 51 for all measures except VO, EL, and KE, for which 50 subjects were analyzed (one was excluded because of noise artifacts).
BSA, Body surface area; *FS*, fractional shortening; *MVE*, mitral valve E velocity.

Table 3 TQ correlations

Parameter	r	*P*
Age	0.36	.09
BSA	0.40	.04
HR	0.53	.00
PRF	0.58	.00

BSA, Body surface area; *HR*, heart rate.

velocity field.[22] This flow feature is demonstrated in Figure 8E, in a patient with a ventricular septal defect (VSD) and double-outlet right ventricle. The strength of the VO field is highest around the VSD. Flow EL has been introduced as a measurement of cardiac efficacy, derived from the spatial gradients of the velocity vector field.[13,21] To illustrate the future potential with BST, the EL measurements of the same patient are displayed in Figure 8F. The EL in this case is highest around the outflows and in the VSD. A map of the KE during right-to-left flow in the VSD is displayed in Figure 8G (see also Supplemental Video 6 available at www.onlinejase.com). A scatterplot displaying how the maximum LV diastolic VO, EL, and KE are associated with age in 50 (of 51) healthy control subjects is presented in Figure 9. One subject was excluded because of noise artifacts. The LV maximum diastolic EL and KE are correlated with age ($r = 0.72$ and $r = 0.73$, respectively); the values increase with increasing age. For VO the relationship with age is less clear. In general, the VO, EL, and KE measurements have high variance, as displayed in the scatterplots (Figure 9). The mean maximum LV diastolic VO, EL, and KE with SDs for the healthy control subjects are given in Table 2.

In Figure 10 and Supplemental Videos 7 and 8 (available at www.onlinejase.com), we demonstrate how flow properties change with changes in LV function over time, from diagnosis to postoperative follow-up of a patient with coarctation of the aorta. The upper images (Figures 10A–10D) demonstrate vortex formation in the apical region that persisted throughout the cardiac cycle when LV function was significantly decreased, on first admission to the hospital. Ventricular function gradually improved after surgical repair, which coincided with changes in flow patterns. The vortex formation was seen more centrally in the ventricle and did not persist throughout the cardiac cycle (Figures 10E–10H) 4 months postoperatively.

DISCUSSION

This is the first study to investigate the clinical feasibility and accuracy of BST. We demonstrated that BST is feasible for pediatric and fetal imaging and provides additional information of blood flow not assessable by traditional CDI. In vitro validation of the method demonstrated accurate velocity measurements down to ≥8 cm in depth. In vivo, BST measures lower velocities compared with PW Doppler, but the BST velocity estimates are highly dependent on smoothing settings. We introduced a TQ map that can provide the user with an important measure of reliability. This map helps identify areas in which the tracking measurements are suboptimal. In addition to calculating the TQ map, an overall subjective quality assessment was performed, with a focus on the quality of the flow visualization.

Possible clinical use of the methodology was illustrated by selected patient examples. We were able to visualize and quantify vortex formations in the right ventricle near VSDs, altered flow patterns in ventricles with reduced function, circular flow near valvar stenosis, and abnormal flow vortices in the pulmonary artery in patients with pulmonary hypertension. We believe that this representation of flows provides a better visualization of preferential flow in complex congenital disorders such as double-outlet right ventricle, as displayed in Figure 8.

Conventional CDI can only measure velocities along the ultrasound beam. The visualization of complex flow patterns using CDI is therefore limited, and assumptions regarding the flow properties must be made. Furthermore, when the Nyquist limit is reached, aliasing artifacts occur, obscuring the true direction of flow.[26] Several approaches for angle-independent velocity estimations have been proposed.[11-13,15] The contrast-based speckle-tracking method, EPIV, has not been able to correctly track blood motion with higher velocities, as frequently found in cardiac disease.[27] BST is a new approach using ultrafast imaging and direct measurements of the blood velocities. Tracking is done on a high–frame rate sequence of images (acquired at a Doppler PRF, in our study 5–7 kHz), in contrast to EPIV, which is performed on the B-mode sequence (<100 Hz).

Like VFM,[13] BST allows simultaneous visualization of vector flow and CDI, and it is possible to extract quantitative velocity information. BST differs from VFM by providing a direct blood velocity measurement, without physical assumptions. BST also has quality measure built in, which aids the clinician's interpretation of the data. In addition, by including wall motion information, it is possible to reconstruct

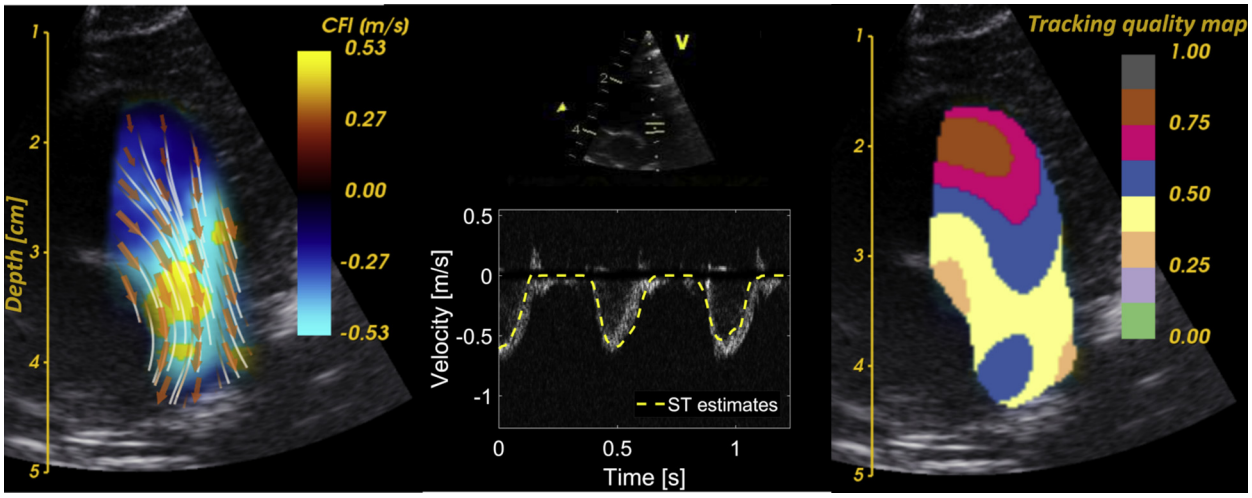

Figure 4 In vivo validation of the 12S probe. Comparison of the velocity estimates from speckle-tracking (ST) toward a PW Doppler signal from the pulmonary artery (sequential recording). BST in the pulmonary artery (*left*), PW Doppler in the middle image, with the ST estimates shown as a *yellow dotted line* superimposed. Corresponding speckle quality map in the pulmonary artery to the right. *CFI*, Color flow imaging.

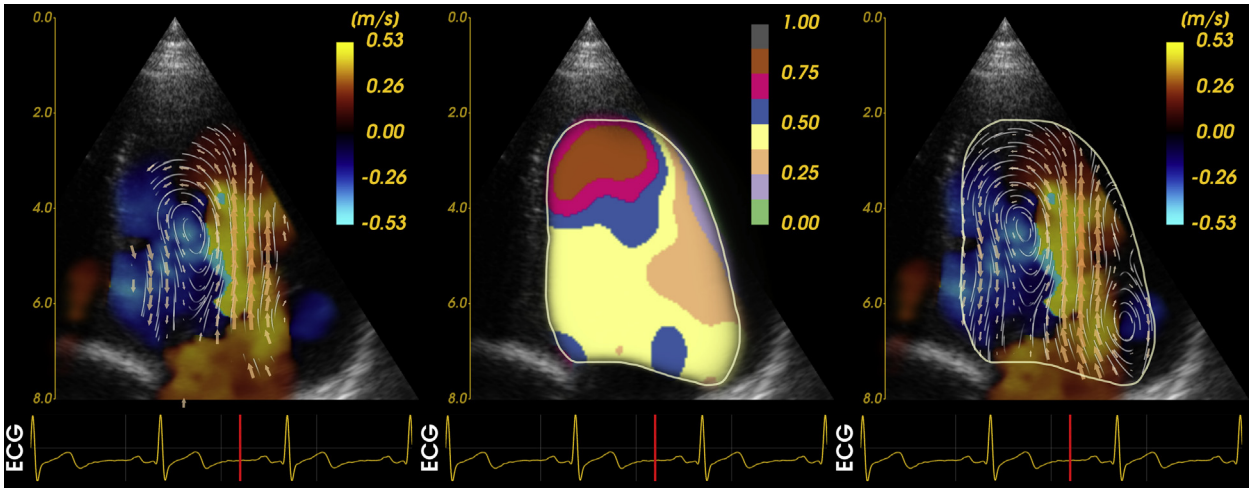

Figure 5 LV flow with and without regularization, with corresponding TQ mapping (6S probe). The image is from a healthy child (9 years old, weight 39.8 kg). BST display is demonstrated to the *left*, the corresponding TQ map in the *middle image*, and on the *right*, cardiac wall information is included to reconstruct missing flow information laterally above the mitral valve. The corresponding Supplemental Video 1 demonstrates domains with CDI (*left*) and regularized BST (*right*) in the left ventricle.

parts of the missing data in dropout regions. This reconstruction can only be trusted when reliable tissue border information can be obtained, and limited out-of-plane flow is present.[24] Contrary to VFM, the wall information is only optional.

Different vortex parameters have been proposed for flow analysis. These include vortex position, area, formation time, duration and relative strength.[28,29] We demonstrated persistent vortex formation in the pulmonary artery in a patient with pulmonary hypertension. Duration of the vortex flow in the main pulmonary artery measured by phase-contrast magnetic resonance imaging correlates linearly with the magnitude of pulmonary hypertension.[30] In addition, alterations in ventricular VO have been observed in pulmonary hypertension.[31] This ability to measure such vortex behavior using ultrasound could have important clinical applications, and this needs to be further evaluated.

Vortex analysis could be an important additional tool for evaluating cardiac function and certainly provides new insights into hemodynamics.[8] Changes in intraventricular flow can be an early marker of reduced ventricular function.[8] In Figure 10, cardiac flow in a dilated left ventricle with reduced function is shown. We demonstrate local stagnation of blood apically, which is previously demonstrated to be associated with an increased risk for thrombus formation.[8,32] We also show how the flow properties changes with improved function.

Vortex visualization in fetal cardiac ventricles (Figure 7B) can possibly contribute to improved understanding and evaluation of cardiac function prenatally. This may be clinically significant because the flow changes are important determinants of fetal morphologic development, remodeling, and epigenetic programming.[4,33] We also believe that BST has the potential to improve prenatal detection of coarctation of the aorta (normal aorta in Figure 7A), which is still a

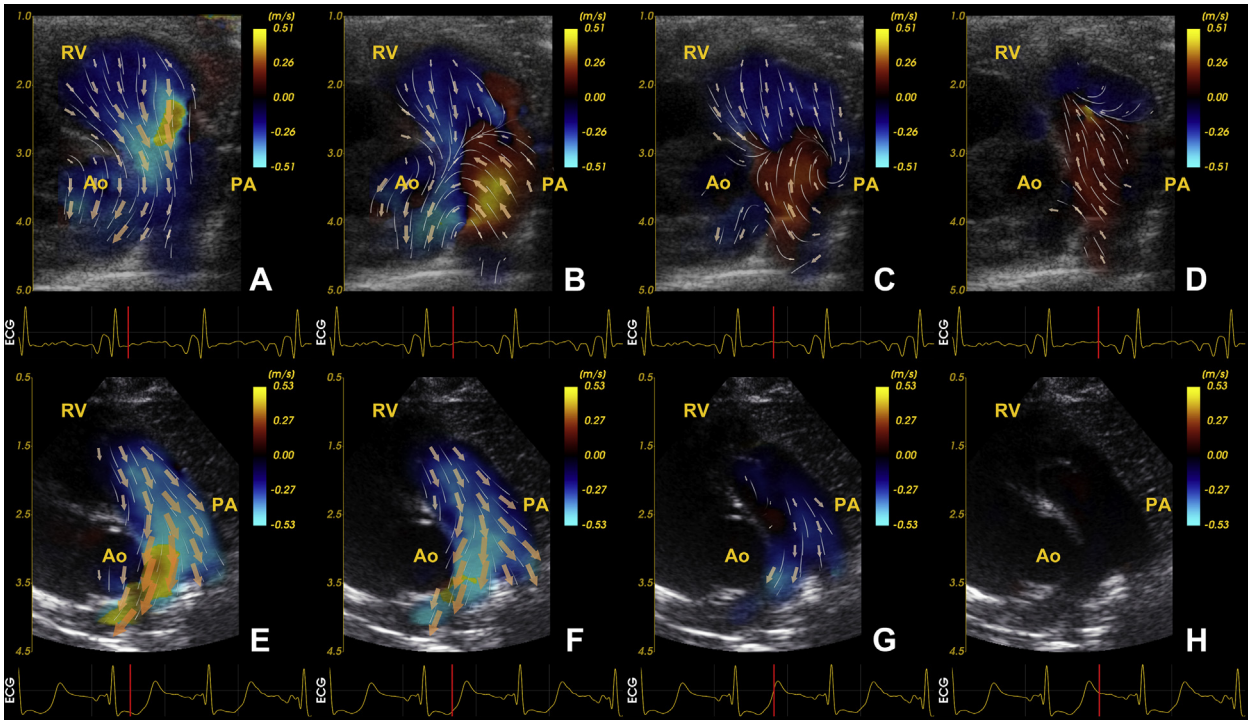

Figure 6 Pulmonary artery flow in pulmonary hypertension. The figure displays still frames from the parasternal short-axis view at four different points in the cardiac cycle. The images demonstrate flow in the pulmonary artery in a size and age matched neonate (3 days, 3.5 kg) with pulmonary hypertension (**A-D** and Supplemental Video 2; 9L probe) and normal pulmonary pressure for age (**E**-**H** and Supplemental Video 3; 12S probe). In the neonate with pulmonary hypertension (100 mm Hg), there is vortex formation in the pulmonary artery visualized by BST **(B, C)**. The vortex persists in 50% of the cardiac cycle. *PA*, Pulmonary artery; *RV*, right ventricle.

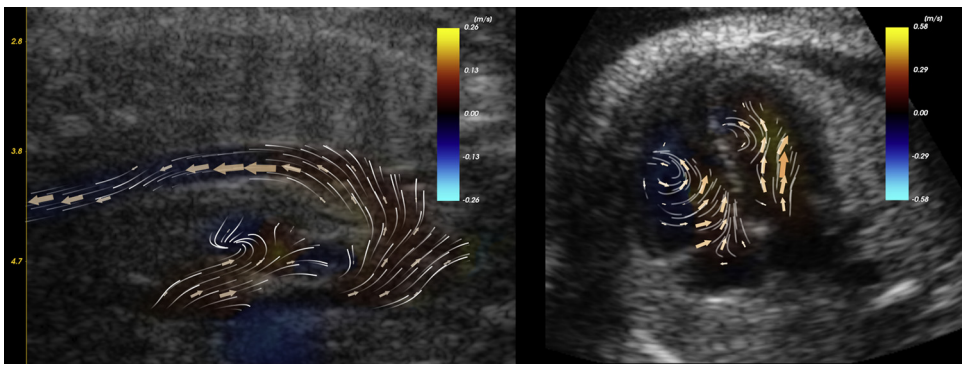

Figure 7 Normal fetus. On the *left*, the aortic arch and descending aorta are shown in a 24-week-old fetus using the 9L linear probe (Supplemental Video 4). On the *right*, a four-chamber view in a 29-week-old fetus is displayed using the 6S probe (Supplemental Video 5).

diagnostic challenge on the basis of conventional fetal imaging.[34] This is a subject for further investigation.

Limitations

The main limitations of ultrafast ultrasound imaging are the reduced penetration and two-dimensional image quality (contrast and resolution). Furthermore, the phased-array transducers have a small aperture with decreasing lateral resolution for increasing depths. This affects tracking accuracy, which decreases with depth and becomes unreliable beyond 9 to 10 cm for the 6S probe. This limits the current application of BST techniques. Furthermore, the high frame rate results in very large raw data files, which is demanding regarding data transfer and storage. Another limitation is signal dropouts, which can occur if there are low radial blood velocities and for pure lateral flows. The PRF can be lowered at the expense of more flashing artifacts to be more sensitive to lower flow velocities. It is also possible to reconstruct the blood velocity fields by using wall information, but this should be done with caution to avoid introducing flow patterns that look physically plausible but do not exist.

We observed that BST measures lower velocities compared with PW Doppler. This can be explained by the fact that the maximum envelope traced around the PW Doppler overestimates the velocity,

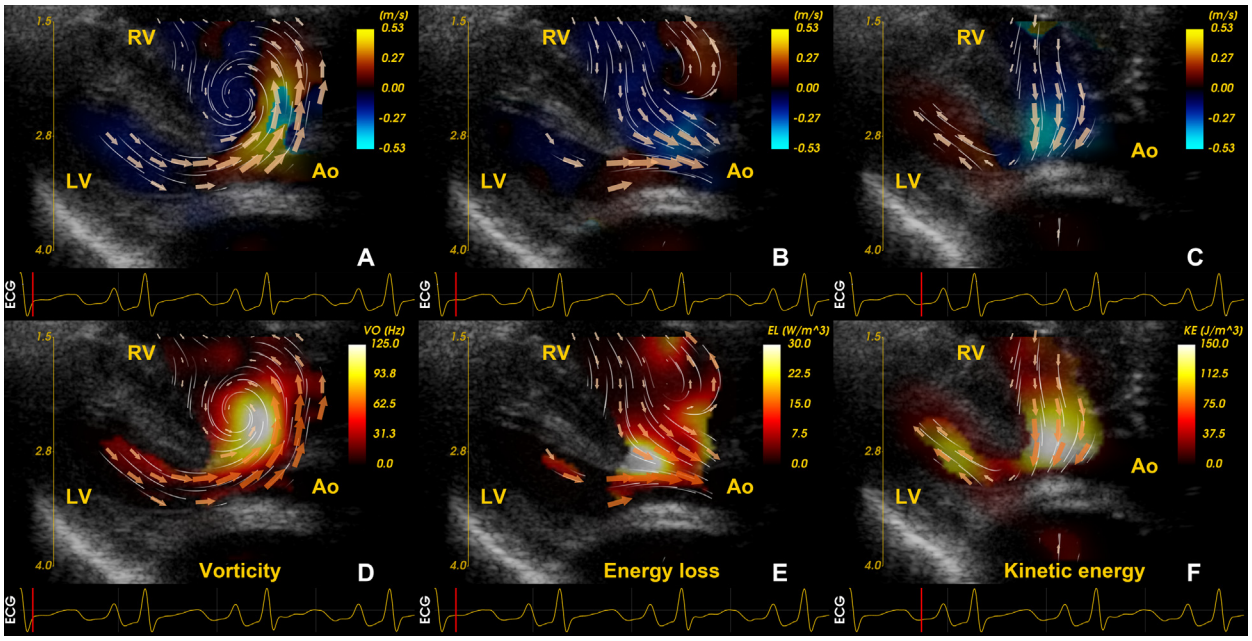

Figure 8 VO, EL, and KE in neonate with double-outlet right ventricle (DORV). The figure displays still frames from the parasternal long-axis view at four different points in the cardiac cycle. The upper panel (A, B, C) displays BST with arrows and streamlines with underlying CDI. The lower panel (D, E, F) displays the corresponding VO, EL, and KE maps. The patient was a 19-day-old neonate (2.5 kg) with DORV, a VSD, hypoplastic mitral valve, and mild pulmonary stenosis. See also Supplemental Video 6. *Ao*, Aorta; *LV*, left ventricle; *RV*, right ventricle.

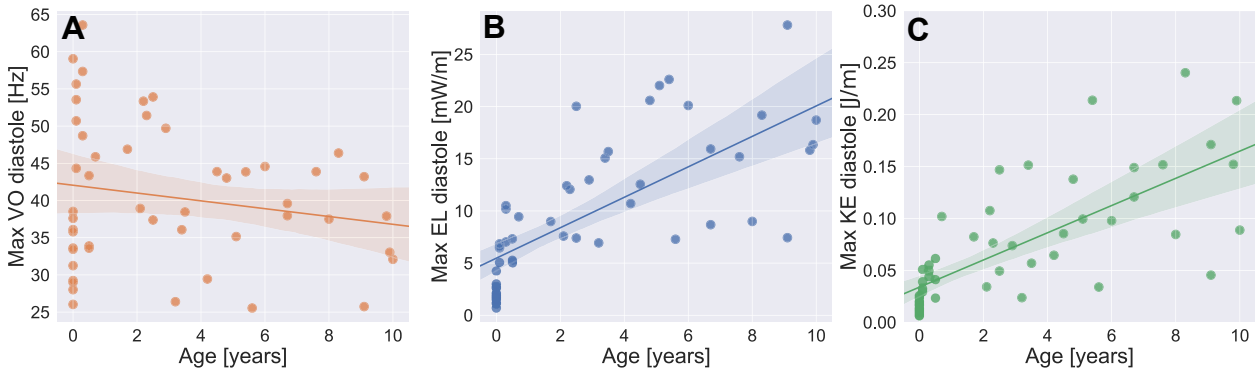

Figure 9 LV VO, EL, and KE. The scatterplots display the relationship between the maximum diastolic VO (**A**, *orange regression line*), EL (**B**, *blue regression line*) and KE (**C**, *green regression line*) with age. The shadowed areas around the lines display the 95% CIs.

while underestimation by BST is present because of spatial and temporal smoothing, as demonstrated in Figure 3A. There is a trade-off between smoothing and noise, and we can improve the maximum velocity estimates, but the data would then be noisier and be less suitable for measures on the basis of the spatial derivatives (e.g., EL).

We describe two-dimensional imaging, but blood flow is inherently three-directional. This means that there may still be some extra factors to be taken into consideration when there is substantial out-of-plane flow. An in vivo example of three-dimensional BST developed in our group was recently demonstrated in a healthy adult.[2] However, clinical feasibility requires further evaluation. Another limitation of this work is that it does not include reproducibility and interobserver variability testing. With regard to the velocity estimates, those are independent of observer as long as the settings in the software are standardized. Inter- and intraobserver variations will largely concern differences in image acquisition imaging planes, which will be investigated in further research.

Future Perspectives

Further studies will focus more on EL and VO calculations. These are derived from the velocity field through the calculation of spatial derivatives of the velocity field. For this reason, we found it important to start with validation of the velocities. Validation of the VO and EL parameters remains to be studied, together with potential clinical utility of these measures.

CONCLUSION

This study demonstrates the initial experience and potential clinical implications of BST in pediatric cardiology. BST is feasible in fetal and pediatric imaging and provides new information of blood flow not available in the traditional CDI. New information of the flow properties generated by BST may increase our knowledge of physiology and pathology in normal and diseased hearts.

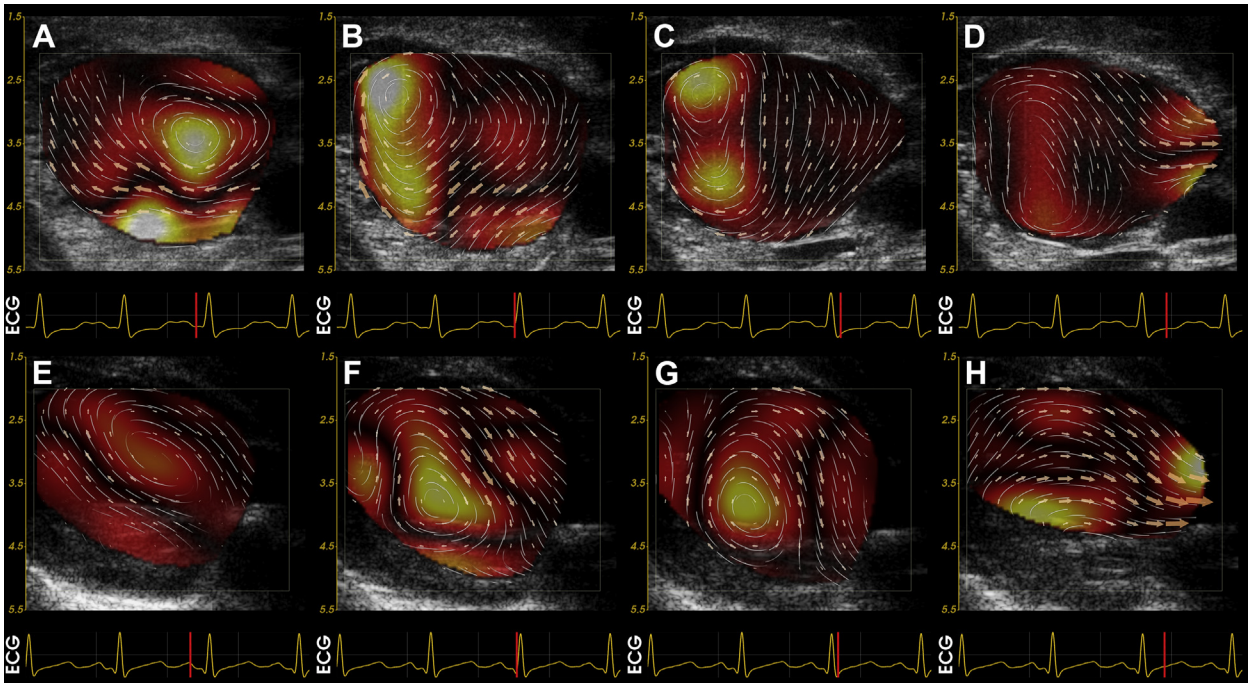

Figure 10 VO map in the left ventricle before and after surgical repair of coarctation of the aorta. Parasternal long-axis view. The patient was 5.5 months old **(A-D)** at diagnosis and 9.5 months old at follow-up **(E-H)**. At diagnosis, there was persistent vortex formations in the apical region (**A-D** and Supplemental Video 7). A pattern such as this will, for example, increase the risk for thrombosis formation. Four months after repair, LV function had normalized, and the vortex formation was more centered in the ventricle and less persistent, with more efficient emptying of the left ventricle (**E-H** and Supplemental Video 8).

ACKNOWLEDGMENTS

We thank Thomas Grønli, MSc, for contributions with the regularization framework. We thank Wendy Williams for copyediting the manuscript. We thank Øyvind Salvesen for statistical advice.

SUPPLEMENTARY DATA

Supplementary data related to this article can be found at https://doi.org/10.1016/j.echo.2019.11.003.

REFERENCES

1. Fadnes S, Nyrnes SA, Torp H, Lovstakken L. Shunt flow evaluation in congenital heart disease based on two-dimensional speckle tracking. Ultrasound Med Biol 2014;40:2379-91.
2. Wigen MS, Fadnes S, Rodriguez-Molares A, Bjastad T, Eriksen M, Stensaeth KH, et al. 4D intracardiac ultrasound vector flow imaging—feasibility and comparison to phase-contrast MRI. IEEE Trans Med Imaging 2018;37:2619-29.
3. Davies PF. Hemodynamic shear stress and the endothelium in cardiovascular pathophysiology. Nat Clin Pract Cardiovasc Med 2009;6:16-26.
4. Hove JR, Koster RW, Forouhar AS, Acevedo-Bolton G, Fraser SE, Gharib M. Intracardiac fluid forces are an essential epigenetic factor for embryonic cardiogenesis. Nature 2003;421:172-7.
5. Boselli F, Freund JB, Vermot J. Blood flow mechanics in cardiovascular development. Cell Mol Life Sci 2015;72:2545-59.
6. Kilner PJ, Yang GZ, Wilkes AJ, Mohiaddin RH, Firmin DN, Yacoub MH. Asymmetric redirection of flow through the heart. Nature 2000;404:759-61.
7. Rodriguez Munoz D, Markl M, Moya Mur JL, Barker A, Fernandez-Golfin C, Lancellotti P, et al. Intracardiac flow visualization: current status and future directions. Eur Heart J Cardiovasc Imaging 2013;14:1029-38.
8. Pedrizzetti G, La Canna G, Alfieri O, Tonti G. The vortex—an early predictor of cardiovascular outcome? Nat Rev Cardiol 2014;11:545-53.
9. Bahlmann E, Gerdts E, Cramariuc D, Gohlke-Baerwolf C, Nienaber CA, Wachtell K, et al. Prognostic value of energy loss index in asymptomatic aortic stenosis. Circulation 2013;127:1149-56.
10. Ro R, Halpern D, Sahn DJ, Homel P, Arabadjian M, Lopresto C, et al. Vector flow mapping in obstructive hypertrophic cardiomyopathy to assess the relationship of early systolic left ventricular flow and the mitral valve. J Am Coll Cardiol 2014;64:1984-95.
11. Hong GR, Pedrizzetti G, Tonti G, Li P, Wei Z, Kim JK, et al. Characterization and quantification of vortex flow in the human left ventricle by contrast echocardiography using vector particle image velocimetry. JACC Cardiovasc Imaging 2008;1:705-17.
12. Chai P, Mohiaddin R. How we perform cardiovascular magnetic resonance flow assessment using phase-contrast velocity mapping. J Cardiovasc Magn Reson 2005;7:705-16.
13. Garcia D, Del Alamo JC, Tanne D, Yotti R, Cortina C, Bertrand E, et al. Two-dimensional intraventricular flow mapping by digital processing conventional color-Doppler echocardiography images. IEEE Trans Med Imaging 2010;29:1701-13.
14. Hayashi T, Itatani K, Inuzuka R, Shimizu N, Shindo T, Hirata Y, et al. Dissipative energy loss within the left ventricle detected by vector flow mapping in children: normal values and effects of age and heart rate. J Cardiol 2015;66:403-10.
15. Gomez A, Pushparajah K, Simpson JM, Giese D, Schaeffter T, Penney G. A sensitivity analysis on 3D velocity reconstruction from multiple registered echo Doppler views. Med Image Anal 2013;17:616-31.
16. Cikes M, Tong L, Sutherland GR, D'Hooge J. Ultrafast cardiac ultrasound imaging: technical principles, applications, and clinical benefits. JACC Cardiovasc Imaging 2014;7:812-23.

17. Claus P, Omar AMS, Pedrizzetti G, Sengupta PP, Nagel E. Tissue tracking technology for assessing cardiac mechanics: principles, normal values, and clinical applications. JACC Cardiovasc Imaging 2015;8:1444-60.
18. Mele D, Smarrazzo V, Pedrizzetti G, Capasso F, Pepe M, Severino S, et al. Intracardiac flow analysis: techniques and potential clinical applications. J Am Soc Echocardiogr 2019;32:319-32.
19. Nyrnes SA, Lovstakken L, Torp H, Haugen BO. Blood flow imaging-a new angle-independent ultrasound modality for the visualization of flow in atrial septal defects in children. Echocardiography 2007;24:975-81.
20. Fadnes S, Wigen MS, Nyrnes SA, Lovstakken L. In vivo intracardiac vector flow imaging using phased array transducers for pediatric cardiology. IEEE Trans Ultrason Ferroelectr Freq Control 2017;64:1318-26.
21. Akiyama K, Maeda S, Matsuyama T, Kainuma A, Ishii M, Naito Y, et al. Vector flow mapping analysis of left ventricular energetic performance in healthy adult volunteers. BMC cardiovascular disorders 2017;17:21.
22. Pasipoularides A. The heart's vortex: intracardiac blood flow phenomena. Shelton: People's Medical Publishing House USA; 2010.
23. Van Cauwenberge J, Lovstakken L, Fadnes S, Rodriguez-Morales A, Vierendeels J, Segers P, et al. Assessing the performance of ultrafast vector flow imaging in the neonatal heart via multiphysics modeling and in vitro experiments. IEEE Trans Ultrason Ferroelectr Freq Control 2016;63:1772-85.
24. Grønli T, Smistad E, Nyrnes SA, Gomez A, Lovstakken L. Reconstruction of in vivo flow velocity fields based on a rapid ultrasound image segmentation and B-spline regularization framework 2016. IEEE Internat Ultrasonics Symp 2016;1-4.
25. Angelelli P, Snare SR, Nyrnes SA, Bruckner S, Hauser H, Løvstakken L, et al. Live ultrasound-based particle visualization of blood flow in the heart. In: Proceedings of the 30th Spring Conference on Computer Graphics. Smolenice, Slovakia: Association for Computing Machinery; 2014. 13-20.
26. Ferrara K, DeAngelis G. Color flow mapping. Ultrasound Med Biol 1997; 23:321-45.
27. Prinz C, Faludi R, Walker A, Amzulescu M, Gao H, Uejima T, et al. Can echocardiographic particle image velocimetry correctly detect motion patterns as they occur in blood inside heart chambers? A validation study using moving phantoms. Cardiovascular ultrasound 2012;10:24.
28. Sengupta PP, Pedrizzetti G, Kilner PJ, Kheradvar A, Ebbers T, Tonti G, et al. Emerging trends in CV flow visualization. JACC Cardiovasc Imaging 2012;5:305-16.
29. Hong GR, Kim M, Pedrizzetti G, Vannan MA. Current clinical application of intracardiac flow analysis using echocardiography. J Cardiovasc Ultrasound 2013;21:155-62.
30. Reiter G, Reiter U, Kovacs G, Olschewski H, Fuchsjager M. Blood flow vortices along the main pulmonary artery measured with MR imaging for diagnosis of pulmonary hypertension. Radiology 2015;275:71-9.
31. Fenster BE, Browning J, Schroeder JD, Schafer M, Podgorski CA, Smyser J, et al. Vorticity is a marker of right ventricular diastolic dysfunction. Am J Physiol Heart Circ Physiol 2015;309:H1087-93.
32. Carlhall CJ, Bolger A. Passing strange: flow in the failing ventricle. Circ Heart Fail 2010;3:326-31.
33. Hill JA, Olson EN. Cardiac plasticity. N Engl J Med 2008;358:1370-80.
34. Wang H, Lei W, Liu J, Yang B, Li H, Huang D. The diastolic and systolic velocity-time integral ratio of the aortic isthmus is a sensitive indicator of aortic coarctation in fetuses. J Am Soc Echocardiogr 2019;32:1470-6.

SUPPLEMENTAL TECHNICAL MATERIALS

Definitions

Tracking Quality. The TQ measure is calculated from the pattern-matching criterion, which was the sum of squared differences in our case. It is given as

$$TQ = 1 - \frac{\min(SSD)}{mean(SSD)}$$

and measures how specific and distinct the best sum of squared differences match is compared with the average, which is linked to the certainty of having a good match. TQ is normalized from [0, 1], where 1 is a perfect match and 0 is a highly uncertain match.

Energy Loss

The EL parameter is related to viscous losses in the fluid, as determined by shear forces and intrinsic fluid viscosity. This is a three-dimensional measurement in watts. However, in two dimensions, we assume only planar shear forces and integrate over the area, which means that the unit is watts per meter. Although the parameter has a relation to viscous EL, we can also consider it as a measure of complexity of the blood velocity vector field compared with a baseline. It is defined in two dimensions as

$$EL = \mu \int 2\left(\frac{\partial v_x}{\partial x}\right)^2 + 2\left(\frac{\partial v_y}{\partial y}\right)^2 + \left(\frac{\partial v_x}{\partial y} + \frac{\partial v_y}{\partial x}\right)^2 dA,$$

where $v = [v_x, v_y]$ is the blood velocity vector, $\mu = 0.004\ Pa/s$ is the blood viscosity, and dA is the area of integration (i.e., color Doppler or LV mask).[21]

Kinetic Energy

The KE of blood is the energy it possesses due to its motion. It is given by the equation

$$KE = \frac{1}{2}\rho v^2,$$

where $\rho = 1060\ kg/m^3$ is the density of blood, and v is the velocity magnitude.

Vorticity

VO measures the rate of rotation around each point in the image. It is calculated by the curl of the blood velocity vector field, which in two dimensions and in absolute value is calculated as

$$VO = |\vec{\omega}| = \left|\frac{\partial v_y}{\partial x} - \frac{\partial v_x}{\partial y}\right|.$$

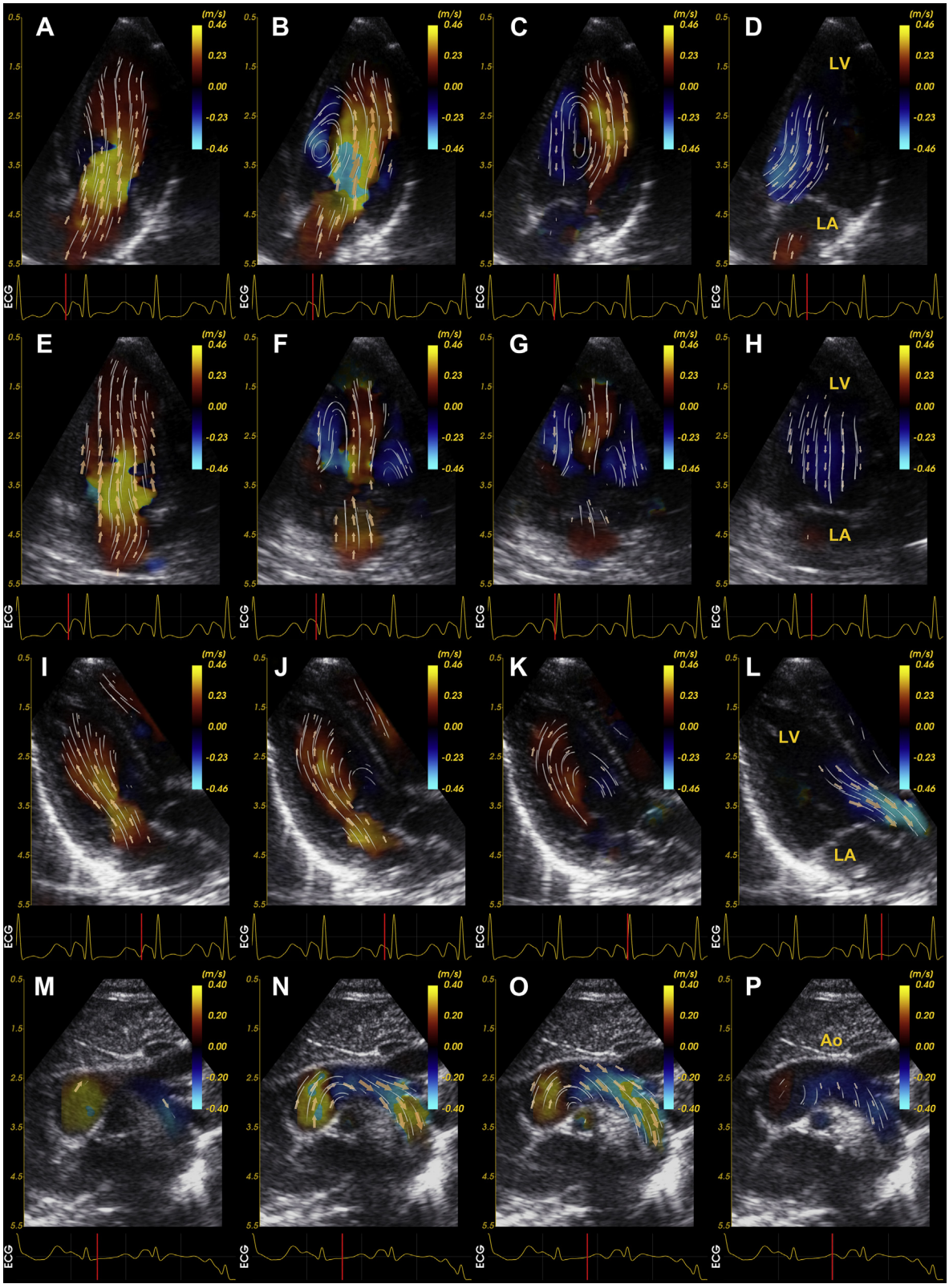

Supplemental Figure 1 Left-sided flow patterns and velocities in a healthy neonate (10 days, 3.8 kg). The figure displays still frames at four different time points in the cardiac cycle. Normal flow properties in the left ventricle; the apical four-chamber view is displayed in **(A)** through **(D**; Supplemental Video 9; the same view is displayed side by side with CDI in Supplemental Video 10 and with regularization in Supplemental Video 11). In Supplemental Video 12 the video with regularization (domain in white) is shown side by side with CDI. The left ventricular two-chamber and three-chamber views are displayed in **(E)** through **(H**; Supplemental Video 13) and **(I)** through **(L**; Supplemental Video 14), respectively. Flow at the corresponding time points in the aortic arch is displayed in **(M)** through **(P**; Supplemental Video 15). Videos are available at www.onlinejase.com. *Ao*, Aorta; *LA*, left atrium; *LV*, left ventricle.

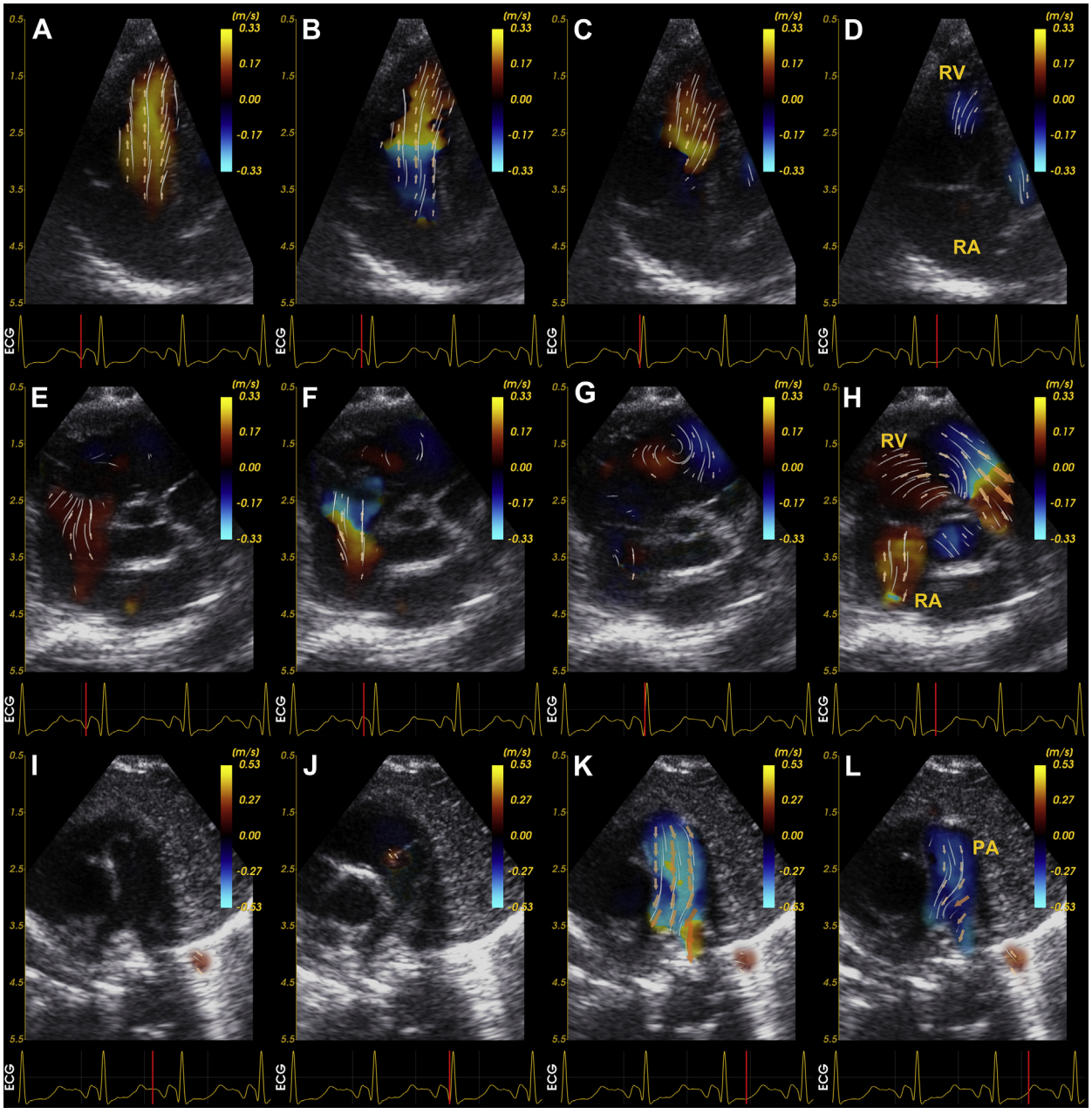

Supplemental Figure 2 Right-sided flow patterns and velocities in a healthy neonate (10 days, 3.8 kg). The figure displays still frames at four different time points in the cardiac cycle. Normal flow properties in the right ventricle seen in the apical four-chamber view (**A–D** and Supplemental Video 16) and the three-chamber view including the right outflow tract (**E–H** and Supplemental Video 17). Flow at the corresponding time points in the pulmonary artery (PA) is displayed below (**I–L** and Supplemental Video 18). Videos are available at www.onlinejase.com. *RA*, Right atrium; *RV*, right ventricle.

Supplemental Table 1 Summary of previous technical validation studies for BST

Type of study	Equipment	Main results	Authors (year)
In vitro/in silico		Validation of velocity estimates	
Computer simulations of intraventricular flows, quantitative analysis of BST in the neonatal cardiac setting	Commercial CFD solver, ANSYS Fluent, Field II ultrasound simulation software	Median magnitude underestimation and angular deviation of 28% and 13.5° during systole and 16% and 10.5° during diastole.	Van Cauwenberge *et al.* (2016)[23]
Computer straight tube flow simulations: maximal velocity 1 m/sec	Field II ultrasound simulation software, simulated pediatric phased-array probe	Degrading velocity estimation accuracy with depth and steering angle. For steering angle 0°, the velocity underestimation increased from 2% to 7% from depth 4.5–9.5 cm. For steering angle 30°, the increase was from 2% to 15%.	Fadnes *et al.* (2017)[20]
In vitro rotating tissue-mimicking phantom: maximal velocity 1 m/sec	GE Vivid E95 scanner with research software, 4V probe	The tracking output was consistent with the ground truth, but an underestimation was observed for higher lateral velocities, in especially in the elevation direction (y direction).	Wigen *et al.* (2018)[2]
In vivo samples		Proof of principle	
BST validation toward color flow imaging and PW Doppler with manual angle correction, shunt flow evaluation	SonixMDP ultrasound scanner (Ultrasonix, Richmond, BC, Canada), 4- to 9-MHz linear transducer	One pediatric patient with VSD, one with ASD (neonates). BST could provide accurate estimates of shunt flow velocities.	Fadnes *et al.* (2014)[1]
Evaluation of the particle animation technique used in BST	GE Vivid E9 scanner with research software, 9L and 11L probes	Two pediatric patients (neonates). Technical description of the integrated method for the acquisition, processing and visualization of live, in vivo blood flow in the heart.	Angelelli *et al.* (2014)[25]
Evaluation of a real-time segmentation framework including definition of flow domains	GE Vivid E9 scanner with research software, 6S and 12S probes	Two pediatric patients. Demonstration of the processing pipeline for reconstructing the flow field in regions of signal dropouts.	Grønli *et al.* (2016)[24]
BST velocities vs in vivo angle-corrected PW Doppler measurements: mitral valve	GE Vivid E9 scanner with research software, 9L and 6S probes	Two pediatric patients. The velocities exceed the Nyquist velocity for the color flow acquisition, but the ST velocity estimates still had a good correspondence with the PW Doppler spectrum.	Fadnes *et al.* (2017)[20]
4D BST: validation against phase-contrast MRI	Modified GE Vivid E95 ultrasound scanner, GE 4V- D matrix-array transducer; Siemens Avanto 1.5-T MRI, software version SyngoB19	One adult subject. Good correspondence between 4D ultrasound BST and phase-contrast MRI regarding quantitative (velocities and velocity-derived parameters such as EL) and qualitative flow analysis (vortex formation).	Wigen *et al.* (2018)[2]

4D, Four-dimensional; *ASD*, atrial septal defect; *BST*, blood speckle-tracking; *CFD*, computational fluid dynamics; *MRI*, magnetic resonance imaging; *PW*, pulsed-wave; *ST*, speckle-tracking.
References correspond to the listed references in the article.

Supplemental Table 2 BSTQ regression analysis: rotating phantom

TQmin, [0, 1]	*r*	RMSE (m/sec)	Data points analyzed	Slope (*a*)	Offset (*b*; m/sec)
0	0.76	0.28	10,000	0.77	0.09
0.1	0.76	0.28	10,000	0.77	0.09
0.2	0.76	0.28	9,800	0.77	0.09
0.3	0.83	0.23	9,490	0.83	0.04
0.4	0.95	0.12	7,100	0.95	0.02
0.5	0.99	0.06	4,600	0.95	0.07
0.6	0.98	0.06	2,600	0.93	0.10

RMSE, Root-mean-square error; *TQmin*, TQ threshold.
Maximum velocity in phantom, 1.5 m/sec; rounds per minute, 285. Slope ($y = ax + b$): slope of regression line; offset ($y = ax + b$), offset of regression line. For TQ = 0.4, $y = 0.95 \times x + 0.02$, where y = BST velocity estimate, and x = ground truth.